Solution Structure of a Trans-Opened (10*S*)-dA Adduct of (+)-(7*S*,8*R*,9*S*,10*R*)-7,8-Dihydroxy-9,10-epoxy-7,8,9,10-tetrahydrobenzo[*a*]pyrene in a Fully Complementary DNA Duplex: Evidence for a Major Syn Conformation

Padmanava Pradhan, Sampath Tirumala, Xiaohong Liu, Jane M. Sayer, Donald M. Jerina, and Herman J. C. Yeh*

Laboratory of Bioorganic Chemistry, National Institute of Diabetes and Digestive and Kidney Diseases, National Institutes of Health, Bethesda, Maryland 20892

Received December 20, 2000; Revised Manuscript Received March 23, 2001

ABSTRACT: Two-dimensional NMR was used to determine the solution structure of an undecanucleotide duplex, d(CGGTC**A**CGAGG)·d(CCTCGTGACCG), in which (+)-(7*S*,8*R*,9*S*,10*R*)-7,8-dihydroxy-9,10-epoxy-7,8,9,10-tetrahydrobenzo[*a*]pyrene is covalently bonded to the exocyclic N^6 amino group of the central deoxyadenosine, d**A**$_6$, through trans addition at C10 of the epoxide (to give a 10*S* adduct). The present study represents the first NMR structure of a benzo[*a*]pyrene (10*S*)-dA adduct in DNA with a complementary T opposite the modified dA. Exchangeable and nonexchangeable protons of the modified duplex were assigned by the use of TOCSY (in D_2O) and NOESY spectra (in H_2O and D_2O). Sequential NOEs expected for a B-type DNA conformation with typical Watson−Crick base pairing are observed along the duplex, except at the lesion site. We observed a strong intraresidue NOE cross-peak between H1′ and H8 of the modified dA$_6$. The sugar H2′ and H2″ of dC$_5$ lacked NOE cross-peaks with H8 of dA$_6$ but showed weak interactions with H2 of dA$_6$ instead. In addition, the chemical shift of the H8 proton (7.51 ppm) of dA$_6$ appears at a higher field than that of H2 (8.48 ppm). These NOE and chemical shift data for the dA$_6$ base protons are typical of a syn glycosidic bond at the modified base. Restrained molecular dynamics/energy minimization calculations show that the hydrocarbon is intercalated from the major groove on the 3′-side of the modified base between base pairs A$_6$-T$_{17}$ and C$_7$-G$_{16}$ and confirm the syn glycosidic angle (58°) of the modified dA$_6$. In the syn structure, a weak A−T hydrogen bond is possible between the N3−H proton of T$_{17}$ and N7 of dA$_6$ (at a distance of 3.11 Å), whereas N1, the usual hydrogen bonding partner for N3−H of T when dA is in the anti conformation, is 6.31 Å away from this proton. The 10(*S*)-dA modified DNA duplex remains in a right-handed helix, which bends in the direction of the aliphatic ring of BaP at about 42° from the helical axis. ROESY experiments provided evidence for interconversion between the major, syn conformer and a minor, possibly anti, conformer.

Polycyclic aromatic hydrocarbons (PAH)[1] are known environmental carcinogens that are constituents of coal tar, soot, and smoke from the incomplete combustion of organic materials such as diesel fuel and tobacco (*1*). Their carcinogenic activity is largely if not entirely due to alkylation of DNA by metabolically formed bay-region diol epoxides (*2*) on angular benzo-rings of the PAH. The exocyclic amino groups of the purine nucleosides, deoxyguanosine (dG) and deoxyadenosine (dA), are the major sites of alkylation (*3*). These diol epoxides exist as pairs of diastereomers in which the benzylic hydroxyl group and the epoxide oxygen are either cis (diol epoxide-1, DE-1) or trans (diol epoxide-2, DE-2). Furthermore, each diastereomer can be optically active. In the case of the hydrocarbon benzo[*a*]pyrene (BaP), the (+)-DE-2 isomer [(+)-(7*R*,8*S*,9*S*,10*R*)-7,8-dihydroxy-9,10-epoxy-7,8,9,10-tetrahydrobenzo[*a*]pyrene] predominates metabolically (*4*) and is the only isomer of the four which is highly tumorigenic (*5*, *6*). Although adducts at dG are *quantitatively* the most significant from this isomer (*7*), the percentage of mutations at dA sites increases substantially when very low, environmentally and physiologically realistic, concentrations of (+)-DE-2 are studied in mammalian cell cultures (*8*, *9*). As far as cell transformation is concerned, the relative importance of adducts or mutations at dA versus dG is unknown. BaP DE adducts have dramatic blocking effects on enzymes such as helicase (*10*) and topoisomerase I (*11*) that are involved in critical aspects of DNA processing in cells, such as replication, repair, and transcription. In particular, BaP DE-2 dA adducts in DNA are potent poisons of topoisomerase I, which permit the normal DNA cleavage step and then irreversibly trap the cleaved DNA−enzyme covalent complex (*11*).

Since diol epoxide adducts are formed by both cis and trans opening of the epoxide at the benzylic position, eight dA and eight dG isomeric adducts are possible. In the case of BaP, the solution structures of oligonucleotide duplexes containing both cis- and trans-opened dG adducts from (+)- and (−)-DE-2 have been established by a combination of NMR techniques and molecular modeling (*12*). For the cis-

* To whom correspondence should be addressed. Phone: (301) 496 4055. Fax: (301) 402 0008. E-mail: hyeh@helix.nih.gov.

[1] Abbreviations: BaP, benzo[*a*]pyrene; PAH, polycyclic aromatic hydrocarbon(s); DE, diol epoxide; rMD, restrained molecular dynamics; EM, energy minimization; IRMA, iterative relaxation matrix analysis.

10.1021/bi002896q
Published on Web 04/27/2001

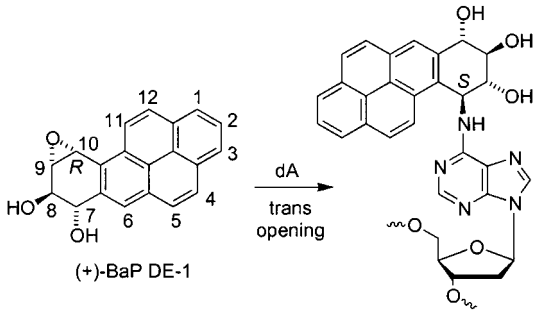

5'-C_1 G_2 G_3 T_4 C_5 **A_6*** C_7 G_8 A_9 $G_{10}G_{11}$-3'
3'-$G_{22}C_{21}C_{20}A_{19}G_{18}T_{17}$ $G_{16}C_{15}T_{14}C_{13}C_{12}$-5'

FIGURE 1: Structures of (+)-(7*S*,8*R*,9*S*,10*R*)-7,8-dihydroxy-9,10-epoxy-7,8,9,10-tetrahydrobenzo[*a*]pyrene [(+)-BaP DE-1] and its (10*S*)-dA adduct in DNA derived from trans opening by the exocyclic N^6-amino group of dA. The sequence of the duplex is also shown (bottom).

opened (10*R*)- and (10*S*)-dG adducts, the hydrocarbons are intercalated with the modified dG and complementary dC displaced out of the helix (*13*, *14*). For trans-opened dG adducts, the hydrocarbons lie in opposite directions in the minor groove (*15*, *16*). All these adducts appear to be conformationally homogeneous in a -C**G**C- sequence context. In the case of dA adducts from BaP, the situation is more complex. Several trans-opened (10*R*)-dA adducts of DE-1 (*17*) and DE-2 (*18*−*21*), as well as a cis-opened (10*R*)-dA adduct of DE-2 (*22*), have the hydrocarbon intercalated. Notably, the only BaP (10*S*)-dA adduct characterized thus far has been in a duplex stabilized by a dG mismatch (*23*). Multiple conformers and/or poorly resolved NMR spectra have precluded determination of the solution conformations of several BaP DE-2 (10*S*)-dA adducts with a complementary T (*20*, *21*, *23*). The present report describes the first NMR structural characterization of a fully complementary duplex containing a (10*S*)-dA adduct of a DE derived from BaP, namely, the trans opened adduct derived from (+)-(7*S*,8*R*,9*S*,-10*R*)-7,8-dihydroxy-9,10-epoxy-7,8,9,10-tetrahydrobenzo[*a*]-pyrene [(+)-BaP DE-1, Figure 1].

MATERIALS AND METHODS

Materials and Sample Preparation. The 11-mer oligonucleotides dCGGTC**A**CGAGG) containing trans-opened adducts of (+)- and (−)-7,8-dihydroxy-9,10-epoxy-7,8,9,-10-tetrahydrobenzo[*a*]pyrene at $\mathbf{A}_6$ were synthesized as a diastereomeric mixture from the protected phosphoramidite using a semi-automated procedure as previously described (*24*); a yield of ∼70% for manual coupling of the modified phosphoramidite was estimated from the amount of dimethoxytrityl cation released on deblocking after the manual step. After 5′-detritylation and removal of base protecting groups, the completed 11-mers were subjected to HPLC on a Hamilton PRP-1 column eluted at 3 mL/min with a linear gradient of acetonitrile in 0.1 M $(NH_4)_2CO_3$ buffer, pH 7.5, that increased the acetonitrile concentration from 5 to 17.5% over 29 min. Under these conditions, our previously reported 11-mer containing the 10*R* adduct (*17*) elutes at 20.9 min, and the isomeric 11-mer containing the 10*S*-adduct that is the subject of the present study elutes at 24.0 min. The late-eluting 10*S* adducted 11-mer was titrated spectrophotometrically (*18*) at 353 nm with its complementary strand to determine the amount required to obtain a 1:1 duplex. The NMR sample (approximately 200 A_{260} units of the duplex) was dissolved in 500 mL of 20 mM sodium phosphate buffer, pH 6.8, in D_2O or H_2O/D_2O 90/10 v/v), containing 56 mM sodium chloride (total ionic strength 0.1 M) and 0.5 mM sodium azide.

NMR Spectroscopy. All NMR experiments were performed on a Varian VXR500 (500 MHz) spectrometer at regulated temperatures. Chemical shifts were referenced relative to a trace of TMSP (sodium 3-trimethylsilyl propionate) at 0.0 ppm. NMR data were acquired without sample spinning. The decoupler and the transmitter offsets were always set equal and on the residual water signal. The residual solvent signal for the D_2O sample was suppressed by presaturating the signal during the relaxation delay. Spectral widths of 6000 and 10 000 Hz were used in both f_1 and f_2 dimensions for the sample in D_2O and H_2O, respectively. The 2D NMR experiments were usually performed in the hypercomplex, phase-sensitive mode (*25*) with 2048 points in the t_2 dimension and 256 t_1 increments with a 3.5 s relaxation delay between scans. NMR data were typically processed using FELIX program (Molecular Simulations, Inc., San Diego, CA [MSI]) with zero-filling in the t_1 and t_2 domain to give 2K × 4K matrixes, respectively, before Fourier transformation. For data processing, a Gaussian or shifted squared sine-bell filter function was used in both dimensions prior to Fourier transformation.

TOCSY experiments (*26*, *27)* with mixing times of 40, 80, and 100 ms were performed on the D_2O sample. NOESY spectra (*28*, *29)* at 5 °C were recorded with mixing times of 40, 80, 160, 200, and 300 ms. One-dimensional ^{1}H spectra for the imino protons were recorded in 10% D_2O at 5 °C and at −10 °C (20% CD_3OD in H_2O) using a modified WET270 pulse sequence (*30*). For assignment of the exchangeable protons, NOESY spectra were recorded at mixing times of 25 and 200 ms at 5 °C, using SWETNOESY (*30*, *31*) with square pulses to improve suppression of residual water. Assignments of H8 and H2 protons of dA_6 (as well as other purine bases) were confirmed on the basis of deuterium exchange experiments (*23*, *32*, *33*). The sample was heated in D_2O at 70 °C for about 30 h, at which time most of the H8 purine protons had exchanged with solvent deuterium, whereas the H2 protons of dA remained unexchanged. ROESY (*34*, *35*) spectra were recorded before and after the deuterium exchange experiment.

Structure Calculations. The structure of the trans-opened BaP DE-1 (10*S*)-dA adducted duplex was calculated by restrained molecular dynamics/energy minimization (rMD/EM) followed by iterative relaxation matrix analysis (IRMA) refinement of the resulting energy-minimized structure to take into account the effect of spin diffusion. The rMD/EM calculations were performed on a Silicon Graphics Indigo O2 workstation using DISCOVER (version 3.0 [MSI]) with the AMBER force field (*36*, *37)*. Partial charges for the adduct in DNA were the same as those employed previously (*23*, *38*). The BaP-modified DNA duplex was built using INSIGHT II (version 98 [MSI]). First a B-type DNA duplex 11-mer was built using the fragments from the standard nucleotide library. A prebuilt 7,8,9-trihydroxy-BaP fragment whose chirality at C7, C8, and C9 corresponded to the parent DE, (+)-(7*S*,8*R*,9*S*,10*R*)-BaP DE-1, was then connected to the exocyclic amino nitrogen of A_6 with 10*S* configuration

Table 1: Restraints Used in the Molecular Dynamics Calculations

NMR restraints	
total distance restraints	254
DNA-BaP distance restraints	14
empirical restraints	
H-bonding distance restraints	28
dihedral planarity restraints	15
chiral restraints	70
H-bonding planarity restraints	38
dihedral restraints	140

at C10 corresponding to trans addition to the 10*R* epoxide. In this starting structure, the hydrocarbon was oriented outside the duplex.

The experimental and empirical restraints utilized for the structural calculations are listed in Table 1. A total of 254 NOE distance restraints, 14 of which were derived from hydrocarbon-oligonucleotide NOE interactions, were employed. These interproton distances were derived from the build-up of NOE cross-peak intensities at 60, 120, 160, 200, and 300 ms. Distance ranges of 1.8−2.5, 2.5−4.0, and 4.0−6.0 Å were set for relatively strong, intermediate, and weak NOE cross-peak intensities, respectively. Watson−Crick hydrogen bonding and planarity restraints were imposed on the basis of the observed NOEs and chemical shifts of imino protons in the duplex DNA. Standard donor−acceptor atom distances (2.6−3.2 Å) for the hydrogen-bonded atoms in B-DNA were used for all base pairs except the adducted dA_6-T_{17} pair; for the two adjacent base pairs these distance restraints were applied with a force constant penalty of 30 kcal mol^{-1} Å^{-2} (50 kcal mol^{-1} Å^{-2} for other base pairs) in the calculations. Additional cross-strand distance restraints were applied for the distance between N3−H (T) and H2 (dA) as well as between N1−H (dG) and N4−H (dC) in the unadducted A−T and G−C base pairs. Since no strong intraresidue base-H1′ cross-peaks were observed, anti conformation for each residue (except for the adducted dA_6) was assumed, and these χ angles were restrained to a range between −70 and −170° (*39*). For all residues except the modified dA_6 and its complementary T_{17}, backbone torsion angles were restrained to ranges (±20° for α, β, γ, ϵ, and ζ; ±30° for δ), which were centered at values derived from X-ray data for standard B-type DNA (*40*, *41*). We think that applying these dihedral restraints was reasonable, since the NMR spectrum was characteristic of a B-type DNA (*39*). Chiral center constraints were applied for the 70 chiral atoms (22 × 3 for sugars and 4 for the tetrahydrobenzo-ring of the BaP DE-1 adduct). For both distances and torsions, force constants of either 30 or 50 kcal mol^{-1} Å^{-2} were used throughout the calculations.

All rMD/EM calculations were done in vacuo with a distance dependent dielectric constant of 4R (with R = the distance between two interacting atoms) and a cutoff distance of 25 Å to simulate the bulk solvent effect. The rMD/EM calculations started at 300 K with a standard B-type duplex DNA structure (see above) with the BaP located completely outside the duplex. Each round of calculation started with 100 iterations of energy minimization with the steepest descents algorithm and with 100 steps (in 1 fs steps) of molecular dynamics without NOE, dihedral angle and base planarity restraints. This was then followed by 2.8 ps of molecular dynamics with restraints on all base pairs except for the central three and during which the temperature was increased to 1000 K. At the highest temperature, molecular dynamics continued for 4 ps in steps of 1 fs, during which full restraints were introduced with a scaling factor of 0.001 in the first picosecond, 10 times greater in the next picosecond, etc. In the fourth picosecond, restraints were in full effect (scaling factor of 1.0). Then the temperature was decreased to 300 K over 7 ps. Finally, 400 iterations of minimization with the steepest descents algorithm and up to 5000 iterations of minimization with the conjugate gradient algorithm were applied to the coordinates derived from each rMD run with no cutoff distances applied for nonbonded interactions. Convergence was determined when the derivative of the force fell below 0.001 kcal/mol.

Structures with the least significant restraint violations (NOE violations <0.1 Å and dihedral angle violations <10°) and relatively low energies in rMD/EM calculations were used as the starting structures in the iterative relaxation matrix analysis (IRMA) calculations (*42*, *43*). Typically, rMD of 5 ps (with a 1 fs step) and 5000 iterations of energy minimization were used in the IRMA calculations. Only NOE distance restraints originating from well-defined, nonoverlapping cross-peaks were used in the IRMA calculations. Several *R* factors, in analogy to the forms described by Gonzalez et al. (*44*), were calculated after each IRMA cycle, including linear, quadratic, and distance-like ($A_{ij}^{1/6}$) forms. The *R* factors decrease in magnitude as the structure refinement progresses and usually converge within two to three cycles. We monitored the distance-like ($A_{ij}^{1/6}$) *R* factor (*23*) in each IRMA cycle. This process was terminated when the *R* factor failed to drop significantly over several iterations.

RESULTS

UV Characteristics and Thermal Stability. The UV absorption maximum for the pyrene chromophore in the present 10*S* adducted oligonucleotide shifts only ∼1 nm (from 352 to ∼353 nm) upon titration of the single stranded oligonucleotide with its complementary strand to give a duplex, as compared to a red shift of 3−4 nm on titration of the isomeric 10*R* adducted oligonucleotide (data not shown). The T_m (*17*) for the present 10*S* adducted duplex is 38 °C under spectrophotometric conditions (10 mM total strand concentration). Thus the temperature of 5 °C used for most of the present NMR experiments is well below the T_m. There is little change in the UV spectrum (data not shown) upon cooling the *duplex* from 25 to −10 °C (20% MeOH in the NMR buffer) and hence no UV evidence for any major temperature-dependent conformational change of the duplex upon further cooling below its T_m.

Exchangeable Protons. The WET270 1D spectrum of the DE-1 (10*S*)-dA adducted 11-mer duplex in H_2O/D_2O at 1 °C (Figure 2) showed eight distinct imino resonances which could be assigned to all the base paired imino protons of dG and T except those of the terminal and central base pairs. The imino proton of T_{17} directly opposite the modified dA in the present (10*S*)-dA adduct is not detected even at temperatures down to 1 °C. This resonance (10.6 ppm) and two other terminal imino resonances (Figure 2, top), however, become discernible on lowering the temperature to −10 °C (20% CD_3OD in H_2O) as the motion/exchange becomes slower on the NMR time scale. This suggests that the conformation of the (10*S*)-dA adduct, in particular, at the

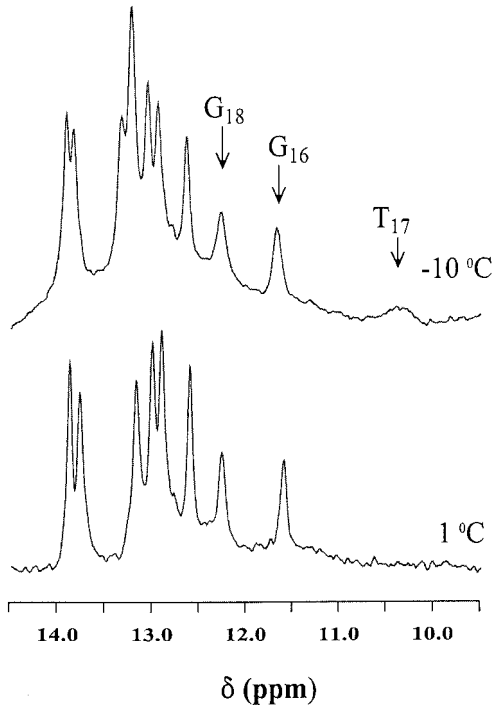

FIGURE 2: Imino proton spectra (10−14 ppm) of the (10*S*)-dA adducted duplex at 1 °C (bottom) [20 mM phosphate buffer, pH 6.8, ionic strength 0.1 M (NaCl),10% D_2O)], and at −10 °C (top). The spectrum measured at −10 °C contained the above buffer composition (in H_2O) and CD_3OD in an 80:20 ratio.

adducted site is relatively more flexible than its (10*R*) counterpart and may explain why many other BaP (10*S*)-dA adducts are intractable to structural study by NMR.

Assignments of the eight distinct imino protons as well as the amino protons were made from analysis of a NOESY spectrum (Figure 3). The imino protons, with the exception of the terminal and central imino protons, were sequentially assigned by tracing through the imino-imino cross-peak connectivity (Figure 3, left). Both cytosine amino protons in each dG-dC base pair were identified by their NOE cross-peaks to the imino proton of guanine (Figure 3, right). The lower-field resonance of the two dC amino protons in each dG-dC base pair exhibited a stronger NOE cross-peak to the imino proton of dG and was assigned to the proton involved in Watson−Crick hydrogen bonding. The assigned chemical shifts of these exchangeable protons are listed in Table 2.

Nonexchangeable DNA Protons. Figure 4 shows expanded 200-ms NOESY contour plots in the region for the base protons (δ 6.8−8.6) and sugar H1′ protons (δ 4.9−6.3) and the connectivity pathways for the modified (broken lines) and the complementary strand (solid lines). The sequential connectivities along each strand of the adducted duplex were established on the basis of NOE cross-peaks between the base protons (H6/H8) and their own and the 5′-flanking sugar H1′ (*45*, *46*). The pattern of NOE cross-peak intensity and the connectivity pathway indicated that the duplex adopted a B-DNA conformation except in the modified region. The sequential connectivities were interrupted between H1′ of dG_{16} and H6 of T_{17} and between H1′ of T_{17} and H8 of dG_{18}. The results indicated perturbation of the DNA structure by the hydrocarbon (presumably intercalation) taking place in this region. However, these sequential breaks alone did not permit a distinction between the two possible intercalation sites, namely, between dG_{16} and T_{17} or between T_{17} and dG_{18}. The site of intercalation was determined to be between dG_{16} and T_{17} based on the observation that the hydrocarbon protons H3−H6 exhibited cross-strand NOEs with sugar and base protons of dG_{16} and T_{17}, as well as with the methyl protons of T_{17} (see below). We observed a weak NOE cross-peak from H8 of dG_{18} to H2′ (or H2″) of T_{17}. In contrast, no NOE cross-peak was observed from H6 of T_{17} to the H2′ (or H2″) of dG_{16}, consistent with intercalation between dG_{16} and T_{17}, but not between T_{17} and dG_{18}. We think the absence of an NOE cross-peak between resonances of H1′ of T_{17} and H8 of dG_{18} is probably due to motional broadening in this region.

Two *unusual* spectral features involving the base protons of modified dA are noted for the present adduct duplex. These are the relatively higher field chemical shift for H8 (δ 7.57 ppm) than for H2 (δ 8.48 ppm) of the modified dA_6 and the relatively stronger cross-peak between H8 and its own H1′ as compared to that for isomeric (10*R*)-dA adducts, whose H8 resonance ($\delta \geq$ 8.4 ppm) generally appears at much lower field than H2 (δ 7.6−8.0 ppm) (*17*, *19*−*21*). The assignment of the resonances at 7.57 and 8.48 ppm to H8 and H2 of dA_6, respectively, in the present adduct was confirmed by deuterium exchange (*23*, *32*). The former (higher field) resonance (along with other purine H8 signals) disappeared on heating the sample to 65 °C for 30 h in D_2O buffer. The unusual shift for H8 and the stronger NOE to its own H1′ is consistent with a syn glycosidic torsion angle at the modified dA (cf. ref *23*). The syn conformation is further supported by the observation of a NOE interaction from the H2 (not H8) of the modified dA_6 to its own sugar H3′. In the syn conformation, H2 of the six-membered purine ring is positioned above the sugar ring and in close proximity to H3′. The large downfield shift of H3′ (δ 5.49 ppm) due to deshielding by the proximal six-membered ring is consistent with this orientation. Several NOE interactions from H2 of dA_6 to H5, H6, H2′, and H2″ of dC_7 and H2′ and H2″ of dC_5 were also observed.

Assignments of other sugar protons (e.g., H2′, H2″, and H3′, etc.) were obtained by sequential analysis of NOE connectivities between these sugar protons and the base protons (H6/H8) (see Supporting Information) and from analysis of the TOCSY spectra (not shown). The H2′ and H2″ resonances for each sugar were identified by analysis of NOESY and TOCSY spectra at short mixing times (∼30−40 ms). In right-handed B-type DNA the H1′ exhibits a stronger NOE cross-peak to the H2″ than to the H2′ of its own sugar. Stronger TOCSY cross-peaks between H1′ and H2′ (relative to H2″) of the same sugar are also characteristic of B-DNA (*39*, *45*). All assignments showed self-consistency. The assigned chemical shifts for the nonexchangeable DNA protons are listed in Table 3. Because of severe signal overlapping and poor resolution in the PECOSY spectrum (2−3 ppm region) coupling constants of sugar protons could not be obtained and thus the sugar conformation was not determined.

Hydrocarbon Protons. Chemical shifts of the hydrocarbon protons for the present (10*S*)-dA adduct were assigned by analyses of the TOCSY and NOESY spectra. The TOCSY spectrum establishes the through-bond connectivities for a three-spin (H1, H2, and H3) and two two-spin (H4 and H5; H11 and H12) systems for the aromatic protons, and a four-

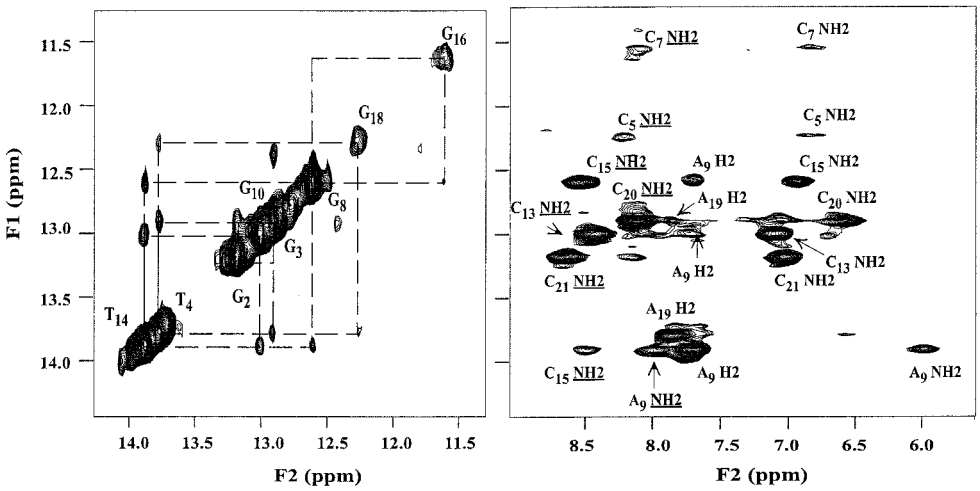

FIGURE 3: Expanded 200 ms NOESY contour plots of the (10*S*)-dA adducted duplex at 1 °C for the imino-imino protons (left) and for the imino-amino and imino-base protons (right). Buffer conditions are the same as for Figure 2 at 1 °C.

Table 2: ^{1}H Chemical Shift Assignments for the Exchangeable Protons in the Base Pairs in the 11-mer Duplex Containing the trans-Opened BaP DE-1 (10*S*)-dA Adduct

base pair	imino H1(dG)/H3 (T)	NH_2 (dC or dA)
C_1-G_{22}	13.06[a]	8.19, 6.91
G_2-C_{21}	13.12	8.59, 7.00
G_3-C_{20}	12.85	8.06, 6.54
T_4-A_{19}	13.73	
C_5-G_{18}	12.28	8.16, 6.82
A_6-T_{17}	10.60[a]	
C_7-G_{16}	11.49	8.03, 7.23
G_8-C_{15}	12.52	8.46, 6.89
A_9-T_{14}	13.82	7.90, 5.89
$G_{10}-C_{13}$	12.96	8.36, 7.07
$G_{11}-C_{12}$	13.06[a]	7.85, 6.98

[a] Observed at −10 °C in 20% CD_3OD.

spin system (H7−H10) for the aliphatic protons. The NOESY data provided additional through-space connectivity between adjacent spin systems. This includes connectivity from H1 to H12, H3 to H4, H5 to H6, H6 to H7, and H10 to H11. Figure 5 displays the expanded NOESY contour plot for the BaP aromatic protons. Chemical shift assignments for the hydrocarbon protons are listed in Table 4.

NOEs between BaP and DNA. Detailed analysis of NOESY spectra in D_2O showed 14 well-defined cross-peaks between protons in BaP and DNA residues, and these were used for structural calculations. These include NOEs between the BaP aromatic protons and the sugar and base protons of T_{17} (complementary to the modified dA), as well as dG_{16}, which forms part of the C−G base pair on the 3′-side of the modified dA. The BaP H4 and H5 protons showed cross-strand NOEs to H1′, H2′ and H2″ of dG_{16} and T_{17}, and H3 of BaP showed a NOE to H1′ of dG_{16}. NOEs were also observed between the BaP H4, H5, and H6 protons and the methyl protons of T_{17}. Other intermolecular NOEs include weak cross-peaks between the H4 and H5 protons of BaP and H3′ of T_{17}, as well as between H4 of BaP and H8 of dG_{16}. In addition, H2 of dA_6 showed a NOE with H11 of BaP. These NOE cross-peaks, combined with the break in sequential connectivity between dG_{16} and T_{17}, indicate that the hydrocarbon is intercalated between residues dG_{16} and T_{17}.

Evidence for a Minor Conformer. Several cross-peaks in the NOESY spectrum, in particular the cross-peak observed near 8.48 and 7.51 ppm, assigned to H2 and H8 of dA_6, respectively, could not arise from dipolar interaction between these two distant protons (6.5 Å apart). These NOE cross-peaks probably result from chemical exchange between two conformers, since the adducted region is quite flexible as demonstrated by the broad imino signal of T_{17} at very low temperature (−10 °C). For verification, ROESY experiments (Figure 6) were performed before and after deuterium exchange with solvent. Several NOE cross-peaks that had the same phase as diagonal peaks were observed in the ROESY spectrum (Figure 6A), indicating that these were indeed NOE cross-peaks resulting from chemical exchange between two conformers. We observed two extremely close exchange cross-peaks at low field, one between 8.48 and 7.53 ppm and the other between 7.51 and 8.51 ppm, in the ROESY spectrum (Figure 6B) before the deuterium exchange. The latter exchange cross-peak disappeared, however, after the deuterium exchange (Figure 6C). These deuterium exchange results permitted unambiguous assignment of the latter cross-peak to H8, which is chemically more susceptible to exchange with solvent deuterium (*33*). The second cross-peak (Figure 6B), which was unaffected by the deuterium exchange, was attributed to the interconversion between H2 in the major (8.48 ppm) and minor (7.53 ppm) conformers. In a 1D spectrum (predominantly major conformer) after deuterium exchange, the resonance at 8.48 ppm (H2) retained nearly full intensity, whereas the resonance at 7.51 ppm (H8) diminished in intensity. Although severe overlap of signals precluded accurate measurement, we estimate that the minor conformer constitutes less than 5%. Two other noticeable exchange cross-peaks in other regions shown as boxed areas b and c in (Figure 6A) were assigned to H1′ (major 6.18 ppm; minor 6.42 ppm) and H3′ (major 5.49 ppm; minor 4.21 ppm) of dA_6. Chemical shifts for the minor conformer determined from these four exchange cross-peaks are indicated in parentheses in Table 3.

Restrained Molecular Mechanics/Dynamics Calculation and Structure Refinement. Restrained MD/EM calculations were performed on a starting structure with an anti glycosidic torsion angle at the modified dA and with the hydrocarbon positioned outside the duplex. A total of 50 MD runs were performed. Eleven of the computed structures that converged

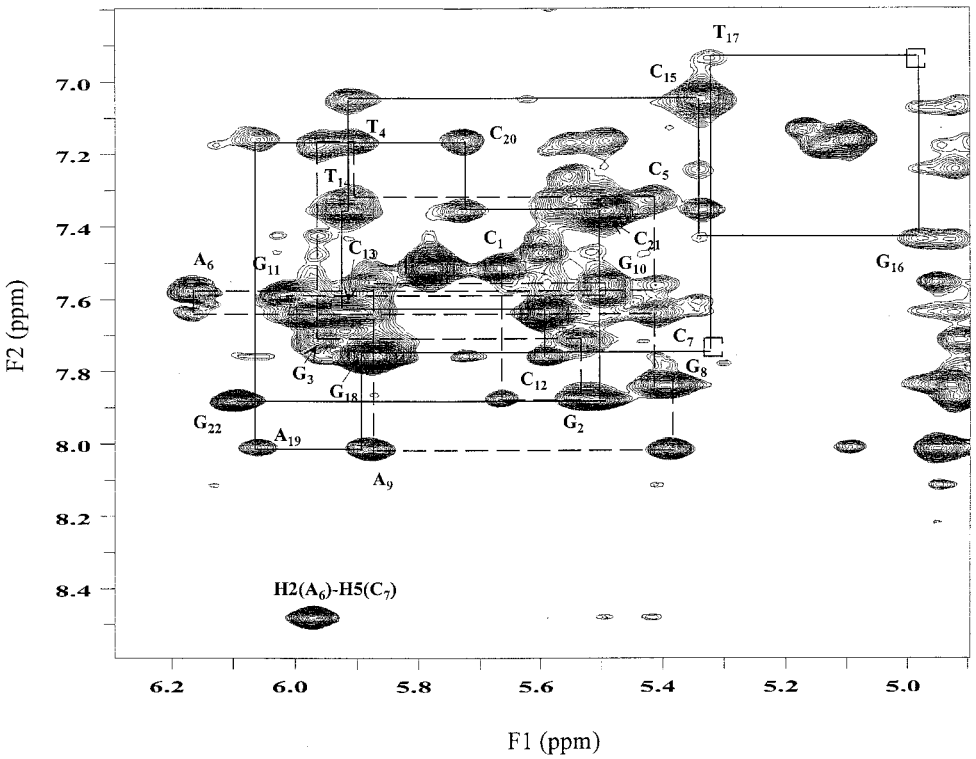

FIGURE 4: Expanded 200 ms NOESY contour plot of the (10*S*)-dA adducted duplex at 5 °C. The downfield shifted H2 resonance of dA_6 (cross-peak to H5 of dC_7) is also shown on the lower-left corner of the plot. Sequential NOE pathways between the base protons (6.8−8.6 ppm) and sugar H1′ protons (4.9−6.3 ppm) for the unmodified and modified strands are shown by solid and broken lines, respectively.

Table 3: ^{1}H Chemical Shift[a] Assignments for Nonexchangeable DNA Protons in the 11-mer Duplex Containing the trans-Opened BaP DE-1 (10*S*)-dA Adduct

		H1′	H2″	H2′	H3′	H4′	H6/H8	H5	H2	M
modified strand										
5′	dC_1	5.67	2.33	1.84	4.63	3.99	7.52	5.79		
	dG_2	5.55	2.69	2.69	4.93	4.27	7.88			
	dG_3	5.97	2.72	2.53	4.89	4.37	7.71			
	T_4	5.91	2.33	1.92	4.74	3.88	7.17			1.30
	dC_5	5.43	1.80	1.31	4.65	3.98	7.32	5.57		
	dA_6	6.18	2.88	2.63	**5.49**	4.28	**7.51**		**8.48**	
		(6.42)[b]			(4.21)		(8.51)		(7.53)	
	dC_7	5.43	2.24	2.00	4.72	4.27	7.65	5.98		
	dG_8	5.40	2.68	2.63	4.96	4.28	7.84			
	dA_9	5.89	2.78	2.57	4.96	4.32	8.02		7.62	
	dG_{10}	5.51	2.56	2.43	4.88	4.25	7.55			
3′	dG_{11}	6.03	2.34	2.25	4.52	4.11	7.59			
complementary strand										
5′	dC_{12}	5.60	2.50	2.24	4.61	3.86	7.76	5.88		
	dC_{13}	5.93	2.45	2.14	4.76	4.17	7.63	5.61		
	T_{14}	5.93	2.34	2.03	4.65	4.12	7.35			1.56
	dC_{15}	5.35	1.89	1.48	4.64	3.90	7.05	5.34		
	dG_{16}	4.98	2.60	2.39	4.93	3.95	7.25			
	T_{17}	5.33	2.04	1.71	4.58	4.33	6.94			1.36
	dG_{18}	5.90	2.33	2.22	4.64	3.72	7.72			
	dA_{19}	6.07	2.76	2.54	4.89	4.30	8.01		7.78	
	dC_{20}	5.74	2.29	1.88	4.69	4.06	7.16	5.12		
	dC_{21}	5.51	2.26	1.91	4.75	3.90	7.35	5.51		
3′	dG_{22}	6.11	2.57	2.31	4.63	4.13	7.88			

[a] Chemical shifts were referenced to TMSP at 0 ppm and HDO signal at 4.88 ppm. [b] The chemical shifts corresponding to the minor conformation are in parentheses.

with NOE violations of ≤0.1 Å and dihedral angle violations of ≤10°, as well as the lowest total energies, had the hydrocarbon positioned 3′ to the modified dA and intercalated between residues dG_{16} and T_{17}. The maximum RMS deviation from the average of these 11 best fit structures was 0.658 Å. These best fit rMD/EM structures were subjected to further IRMA calculations using 121 well-separated NOE cross-peaks. Figure 7 shows the superposition of the IRMA refined structures. As expected, atoms in the backbone showed greater inconsistency than atoms in sugars and bases. A stereoview of the average refined structures is shown in Figure 8. The hydrocarbon shows intercalation between the modified base pair and the base pair on its 3′-side, with the aromatic rings sandwiched between dG_{16} and

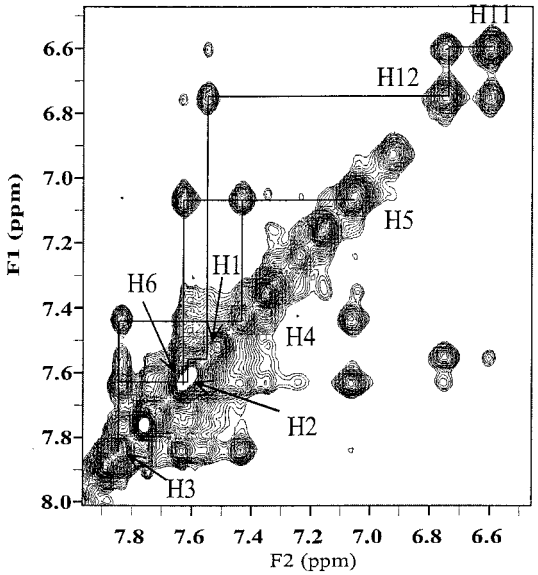

FIGURE 5: Expanded 200 ms NOESY spectrum at 500 MHz showing the assignments for the aromatic protons of BaP.

Table 4: Chemical Shift Assignments[a] for Protons of the Hydrocarbon Moiety in the BaP DE-1 (10*S*)-dA Adduct

proton	chemical shift (ppm)	proton	chemical shift (ppm)
H1	7.56	H7	4.72
H2	7.63	H8	3.63
H3	7.84	H9	3.87
H4	7.44	H10	5.60
H5	7.08	H11	6.61
H6	7.64	H12	6.76

[a] Referenced to TMSP at 0 ppm and HDO signal at 4.88 ppm.

T_{17}. The most notable structural feature of the present adduct is the syn glycosidic angle (58°) of the modified dA_6.

DISCUSSION

Although several studies from this laboratory (*17*, *21*) and others (*19*, *20*, *22*) have described the use of NMR to determine solution structures of fully complementary oligonucleotide duplexes containing BaP DE adducts at the N^6 amino group of dA, these reports have been limited to adducts with 10*R* configuration at the point of attachment of the hydrocarbon to the adenine base. The diastereomeric 10*S* adducts, which are of considerable biological interest since one such adduct is the product of trans ring opening of the most carcinogenic (*R*,*S*,*S*,*R*)-DE-2 isomer, have to date resisted elucidation by NMR, most likely as a result of conformational heterogeneity and dynamic motion at the adduct site. Such (10*S*)-dA adducts, derived from either DE-1, DE-2, or 9,10-epoxy-7,8,9,10-tetrahydro-BaP (BaP H_4-E) lacking the 7,8-diol functionality, share characteristics that are consistent with decreased duplex stability and altered stacking interactions relative to their "better-behaved" 10*R* counterparts (*47*). For example, such trans-opened (10*S*)-dA adducts [as well as the cis-opened BaP H_4-E (10*S*)-dA adduct] in the present 11-mer sequence all have T_m values that are 5−8 °C lower than their10*R* counterparts and 14−19 °C lower than the unmodified duplex (T_m 54 °C). On titration with their complementary strands at a temperature well below the T_m, (10*R*)-dA adducts exhibit both an

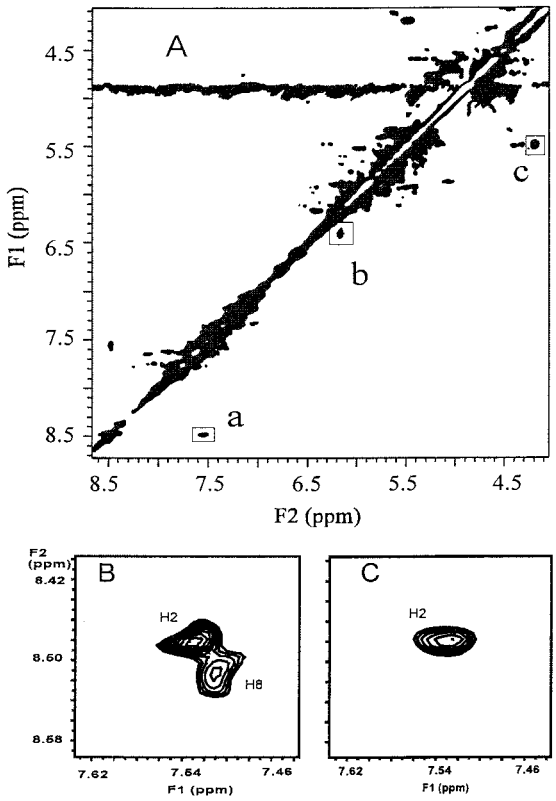

FIGURE 6: Expanded ROESY contour plot (δ 4.0−8.6 ppm, 40 ms mixing time) for the (10S)-dA adducted DNA duplex obtained at 5 °C after deuterium exchange (A). Detail of plot showing NOE exchange cross-peak(s) for the base proton(s) (box a in panel A) of the modified dA_6 before (B) and after (C) the deuterium exchange.

absorbance decrease and a 3−7 nm red shift of the long-wavelength pyrene band at ~350 nm accompanying duplex formation. In contrast, (10*S*)-dA adducts exhibit comparable absorbance decreases but small or negligible (≤2 nm) red shifts. Similar effects of 10*S* vs.10*R* configuration are also apparent for analogous DE-2 and H_4-E dA adducts in other sequence contexts (*21*, *47*).

The present report constitutes the first successful structure determination by 2-dimensional NMR techniques of a fully complementary DNA duplex containing a (10*S*)-dA adduct of a BaP DE. The adduct in this case results from trans opening of the (+)-(*S*,*R*,*S*,*R*)-DE-1 isomer (Figure 1). The very similar properties of the BaP DE-1, DE-2, and H_4-E adducted duplexes observed on UV spectroscopy, as well as comparison of the current structure with a (10*S*)-dA adduct of DE-2 in a mismatched duplex (see below), suggest that this DE-1 (10*S*)-dA adduct is a reasonable model for the corresponding DE-2 (10*S*)-dA adduct, whose structure to date remains unsolved. The fact that our present 11-mer duplex containing the DE-1 adduct appears to be only slightly more stable thermally (~3 °C higher T_m) than its DE-2 adducted counterpart suggests that very small differences in conformational distributions and/or rates of interconversion may be crucial to the success of these NMR structural studies.

*Structural Features.*The present (10*S*)-dA adducted duplex consists largely but not exclusively of a single conformer whose structure was refined by rMD/EM utilizing NOE distance restraints. Sequential NOE cross-peaks of the present adduct were consistent with a B-type DNA conformation along the duplex, except at the lesion site. The observed

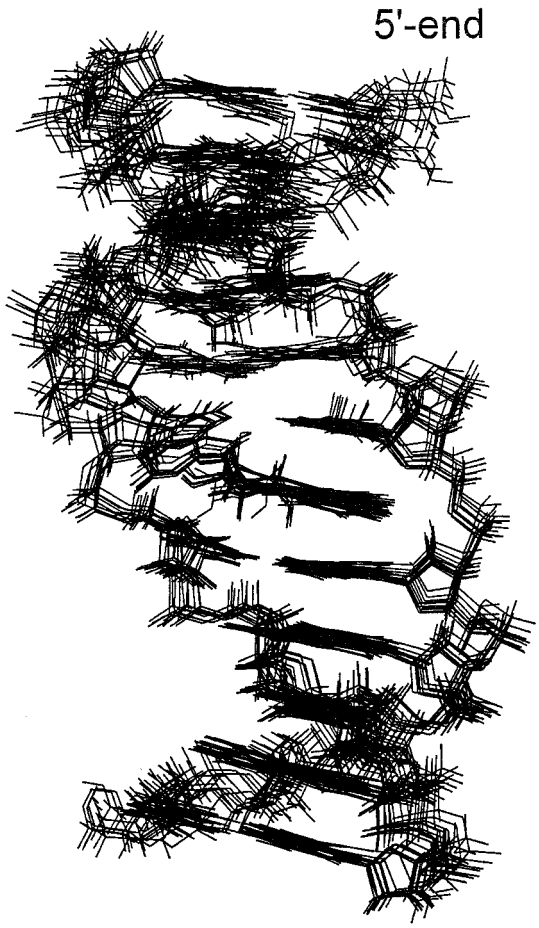

FIGURE 7: Superposition of eleven structures obtained from rMD/EM calculations (rmsd 0.658 Å). The 5′-end of the modified strand is at the top.

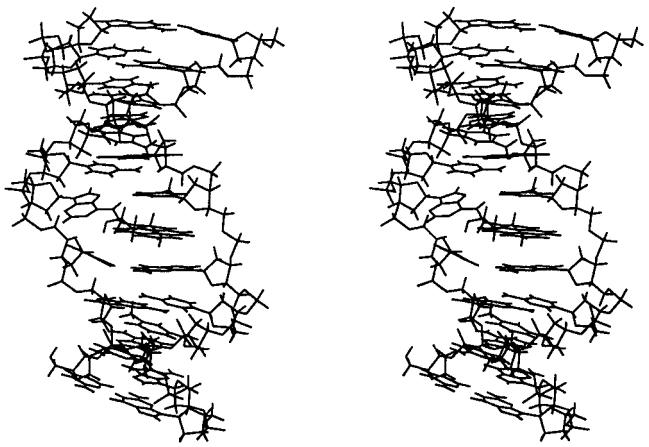

FIGURE 8: Stereoview of the averaged refined structure of the present (10*S*)-dA adducted duplex, looking into the major groove. The 5′-end of the modified strand is at the top.

NOEs indicated that the hydrocarbon was intercalated, consistent with all previous NMR structures (*17*−*23*) for BaP DE adducts at dA. NOE interactions between the hydrocarbon and the nonexchangeable protons of the base pair on the 3′-side relative to the adducted strand established that the aromatic ring system was intercalated 3′ to the modified base. This orientation is similar to that observed for other (10*S*)-dA adducts of DEs derived from BaP (*23*), benzo[*c*]-phenanthrene BcPh) (*48*) and benzo[*a*]anthracene BA) (*49*), and opposite to that observed for the corresponding (10*R*)-dA adducts (*18*−*22*, *50*, *51*).

A stereoview of the final structure for the predominant conformation obtained from the rMD/EM calculations is shown in Figure 8, and comparative views of the central three base pairs of final 11-mer duplexes containing the present trans-opened DE-1 (10*S*)-dA adduct (left) and the corresponding (10*R*)-dA adduct (*17*) (right) are shown in Figure 9. In the present structure, the glycosidic torsion angle at the modified dA_6 is syn. Spectral features of the modified dA_6, such as the high-field shifted resonance of H8 and its strong intraresidue NOE interaction with H1′, as well as the NOE between H2 and H3′, all support this orientation. In the syn conformation, the six-membered ring of dA_6 is positioned over its sugar ring with H2 facing H3′, whereas the five-membered ring points away from the sugar ring and orients N7 within hydrogen bonding distance (3.11 Å) of the N3−H of T_{17}. The syn orientation also places the H2 of dA_6 close to many protons of adjacent residues on both sides of the modified base, namely, H5, H6, H2′, and H2″ of dC_7 and H2′ and H2″ of dC_5. All other glycosidic torsions in the duplex are in the normal *anti* conformation.

The intercalated BaP wedges apart the two bases of dG_{16} and T_{17} of the complementary strand from the typical base-base rise distance (Dz 3.3 Å) to 6.7 Å as determined from Curves (*52*), a program suited for determination of helical parameters of irregular nucleic acids. To accommodate the large rise distance the two bases, dC_7 and dA_6, of the modified strand, buckle at −26 and 30 °C (see Figure 9, left) and form weak base pairs to dG_{16} and T_{17}, respectively. The widening between dG_{16} and T_{17} is also partially compensated by shortening of rise distances of next two adjacent inter-base stacking pairs (Dz 2.4 Å between dG_{15} and dC_{14} and 2.6 Å between T_{17} and dG_{18}). The intercalation together with the glycosidic syn conformation at the modified dA resulted in a Hoogsteen type dA_6-T_{17} base pair (see Figure 10A, left) with about 180° rotation of the base of dA_6 (positive propeller twist, ω, 169°). Values of propeller twist ranging between −4° and −28°, typical for a base pair with anti-anti sugar conformation, have been reported for an unmodified DNA dodecamer (*53*−*55*). The average helical twist is 31.7°, indicating a slight under-winding of the modified DNA (33.2° for the calculated unmodified DNA (*56*)). The (10*S*)-dA modified 11-mer duplex remains in a right-handed helix with a path length of 34.8 Å and end-to-end distance of 32.3 Å. The duplex shows a bend of about 42° from the helical axis in the direction of the aliphatic ring of the hydrocarbon.

The aliphatic ring of BaP is exposed in the major groove, and the aromatic system is intercalated toward the 3′-end of the adducted strand, between the central dA_6-T_{17} and its neighboring base pair (dC_7-dG_{16}). The edge of the hydrocarbon comprising H3, H4, and H5 of the BaP faces toward the major groove, whereas the edge comprising H1 and H12 is inserted through the helix and orients toward the minor groove. Interestingly, the aromatic portion in the trans 10*R* adducted duplex also inserts into the DNA helix with the same facial orientation, with H3, H4, and H5 of the BaP facing the major groove. Since the parent DEs are mirror images, this requires the hydrocarbon of the trans (10*R*)- and (10*S*)-dA adducts to intercalate on opposite sides of the modified base pair, as observed. Potential-energy calculations (*57*) indicate that these opposite spatial orientations of the

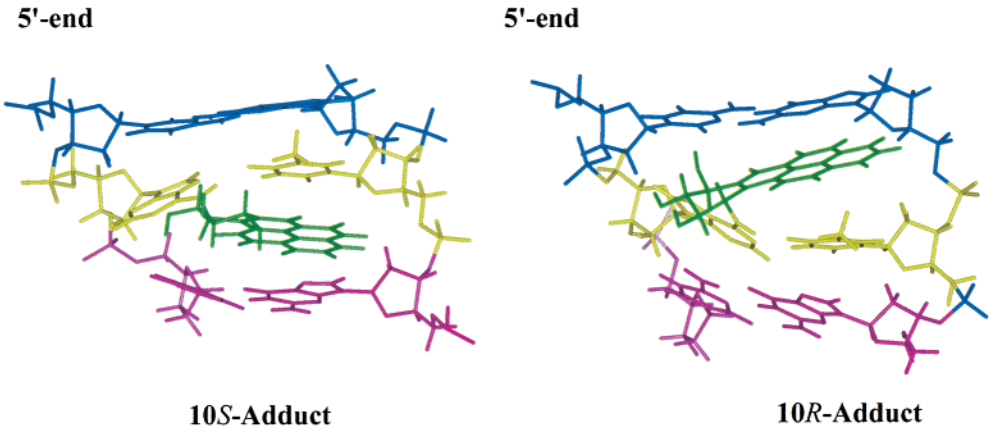

FIGURE 9: Comparative views (looking into the major groove) of the central three base pairs of the present (10*S*)-dA adducted duplex (left) and the isomeric (10*R*)-dA adducted duplex (*17*). Both duplexes contain a T complementary to the adducted dA. The 5′-end of the modified strand is at the top. The hydrocarbon is shown in green, and the C_5-G_{18}, A_6-T_{17}, and C_7-G_{16} base pairs are shown in purple, yellow and magenta, respectively.

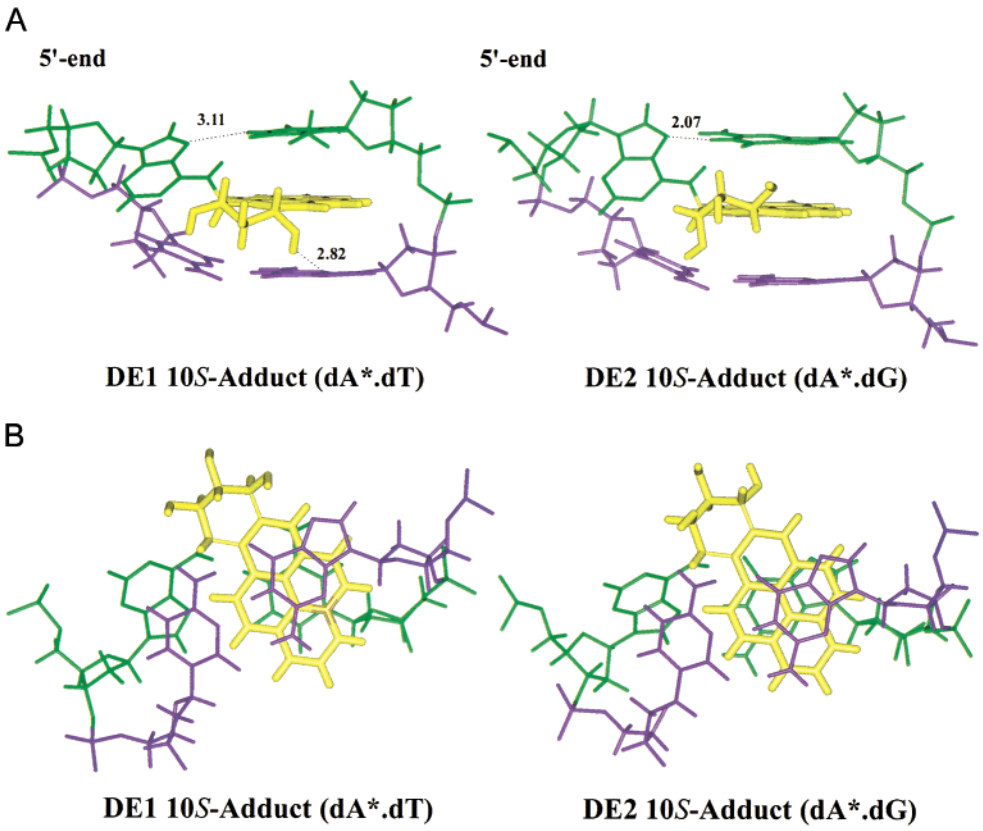

FIGURE 10: Views of the present BaP DE-1 (10*S*)-dA adducted duplex (left) and a BaP DE-2 (10*S*)-dA adducted duplex (right) with a mismatched dG (*23*) opposite the adduct. The hydrocarbon is shown in yellow, and the A−T(G) and C−G base pairs are shown in green and magenta, respectively. (A) View into the major groove. The modified base pair and its neighboring base pair toward the 3′-side of the adducted strand are shown. The 5′-end of the modified strand is at the top. Distances between N7 (A) and N3−H (T) or N1−H (dG) are indicated. (B) View of stacking interactions between the hydrocarbon, the adducted base pair, and the C−G base pair adjacent to the hydrocarbon looking along the helix axis from the 3′-end of the modified strand.

hydrocarbon relative to the adenine base for adducts of the two enantiomeric DEs are also energetically preferred in the monomeric adducts due to steric hindrance. Stacking interactions with the pyrene moiety presumably account for the upfield chemical shifts observed for H6 of T_{17} and H8 and H1′ of dG_{16}. Interestingly, the methyl protons of T_{17} in the present (10*S*)-dA adducted duplex resonate at a near-normal position (1.36 ppm), whereas these protons in the corresponding (10*R*)-dA adducted duplex (*17*) are massively upfield shifted (to −0.2 ppm). In the present structure, this methyl group lies above an edge of the pyrene ring system, whereas in the 10*R* adducted duplex the methyl group is directly below the central portion of the aromatic system (cf. Figure 9). There are also several marked differences in chemical shifts for the BaP moiety between the present (10*S*)-dA adduct and its 10*R* counterpart. Large downfield shifts for H1, H2, and H3 and significant upfield shifts for H5 and H6 are observed in the present 10*S* adduct as compared to the 10*R* adduct. These may result from differences in the spatial arrangement of the two bases flanking the hydrocar-

bon. In the present (10*S*)-dA adduct, the hydrocarbon inserts tightly between T_{17} and dG_{16} such that these bases are positioned directly above and below the center of the aromatic system. In contrast, for the (10*R*)-dA adduct, the two flanking bases (T_{17} and dG_{18}) are slightly offset, and lie above and below H1 and H12.

The conformation of the present duplex is strikingly similar to that of a 9-mer duplex with the same sequence but containing a dG mismatch (*23*) opposite a DE-2 (10*S*)-dA adduct (Figure 10). In both structures, the predominant conformer has a syn glycosidic torsion angle for the adducted adenine base. The hydrocarbon intercalates in such a way that the edge of the pyrene corresponding to H12, H1, and H2 is pushed through the helix and extends into the minor groove. As shown in Figure 10B, the BaP ring in the present duplex is stacked between a pyrimidine (T_{17}) and a purine ring (dG_{16}) whereas in the mismatched duplex, the BaP is sandwiched between two purine rings (one of which is the mismatch) resulting in different stacking interactions but little change in the overall orientation of the pyrene ring system. The T (dG) residue opposite the adducted dA is positioned such that N3−H (T) or N1−H (dG) approaches N7 of the syn dA_6. The short distance (2.07 Å) between N1−H (dG) and N7 (dA) in the mismatched 9-mer (Figure 10A, right) is consistent with hydrogen bonding, whereas in the present case, N3−H (T_{17}) is farther away (3.11 Å) and would thus form a weaker H-bond with N7 (A_6) (Figure 10A, left). The extremely broad signal for the N3−H (T_{17}) proton in the exchangeable proton spectrum of the present duplex (Figure 2, top) contrasts with the sharp resonance for the corresponding dG imino proton signal in the dG mismatch (*23*) and supports this interpretation. Consistent with the similar orientations of the BaP moiety in both the present DE-1 adduct and the DE-2 dA/dG mismatch, differences in chemical shifts for individual aromatic protons in the two structures are ≤0.2 ppm. Upfield shifts for the aliphatic protons H7, H8, and H9 (∼0.3−0.4 ppm) of the present DE-1 adduct presumably reflect the different relative stereochemistry of the DE-1 and DE-2 adducts; in particular, the facial orientations of both H7 and H8 relative to the adenine at H10 are switched in the DE-1 when compared with the DE-2 adduct.

Minor Conformer. We previously demonstrated that the 9-mer duplex described above with a mismatched dG opposite a BaP DE-2 (10*S*)-dA adduct contained ∼17% of a minor conformer whose spectrum was resolvable from the major conformer on the NMR time scale. Interconversion of the major, syn conformer with this minor species, whose structure was solved and shown to have the anti orientation of the glycosidic bond of the adducted dA (*58*), gave rise to chemical exchange cross-peaks. In the present structure, a limited number of analogous chemical exchange cross-peaks involving protons that have large chemical shift differences in the two conformers are observed (Figure 6). The most crucial of these are the two very close but resolvable cross-peaks, between 8.48 and 7.53 ppm and between 8.51 and 7.57 ppm. Isotope exchange of the sample with solvent deuterium unambiguously assigned these peaks to H2 and H8, respectively. On the basis of deuterium exchange and NOESY spectral assignments, it is clear that the farthest downfield signal observed in a 1D NMR spectrum corresponds to H2 of dA_6 in the major (syn) conformer, and that the H8 resonance in this major conformer is shifted far upfield to ∼7.5 ppm. This represents a reversal of the normal chemical shifts observed for these two protons and is typical (*21*, *23*, *49*) of the syn conformation of hydrocarbon-adducted dA in several related oligonucleotides including the mismatched 9-mer described above. The low field signal (8.51 ppm) assigned to H8 of the *minor* conformer is typical for an anti glycosidic conformation but is too small and too close to be resolved from the nearby H2 resonance of the *major* conformer in a 1D spectrum. Hence the percentage of the minor (most likely anti) conformer present could only be estimated (<5%).

Oligonucleotide duplexes containing both (1*R*)- and (1*S*)-dA adducts derived from benzo[*c*]phenanthrene (BcPh) (*48*, *50*) and benzo[*a*]anthracene (BA) (*49*, *51*) DE-2 with a complementary T have been characterized by NMR. Although the 1*R*-adducted duplexes in both cases were conformationally homogeneous (*50*, *51*), the 1*S*-adducts showed the presence of minor conformers (*48*, *49*). For the BA DE-2 (1*S*)-dA adduct, strong evidence was presented for a syn glycosidic torsion at the modified dA in the *minor* (*20%*) *conformer*. The conformational equilibrium is altered for the BaP relative to the BA adduct such that in the present BaP DE-1 (10*S*)-dA adduct, the *major conformer* has this unusual syn conformation. The similarity between the present structure and a BaP DE-2 (10*S*)-dA adduct in which the syn conformation is stabilized by hydrogen bonding to a mismatched dG makes it likely that this conformational motif is also significant for the DE-2 (10*S*)-dA adduct when its complementary base is T. We speculate that a putative hydrogen bond between the 7-hydroxyl group of the BaP moiety and N7 of dG_{16} (cf. Figure 10) in the DE-1 adduct may sufficiently stabilize the major conformation or slow its rate of interconversion with other conformation(s) so that the present NMR analysis was made possible. Because the 7-hydroxyl group is oriented on the opposite face of the ring system in the present DE-1 adduct relative to its DE-2 counterpart, this hydroxyl may approach closely enough (2.82 Å as shown) for hydrogen bonding to N7 of dG_{16} (Figure 10A) in the present adduct, but not in its DE-2 isomer. The success of the present determination, in light of the recalcitrance of the corresponding DE-2 adducts to NMR structural elucidation, highlights the importance of relatively small structural or conformational differences that can influence the rates and equilibria for conformational interconversion.

For PAH DE adducts at dA investigated to date, significant contributions from minor conformers have generally been characteristic of the isomer with *S* configuration at the point of attachment of the hydrocarbon to the adenine base. However, evidence for conformational heterogeneity in some DNA duplexes containing a BaP DE-2 (10*R*)-dA adduct has recently been reported as well (*20*, *21*). Stone and co-workers (*20*) reported a fast dA_6 sugar pucker interconversion (between C2′-endo and C3′-endo conformation) for the base (A) *adjacent to* the modified dA in the local sequence -CA**A***G-. When the adduct was at the alternative A (-C**A***AG-), no evidence for this type of conformational equilibrium was observed (*19*). In another recent study, NOE chemical exchange (*21*) indicated the existence of a minor (≤5%) conformer, probably with a syn glycosidic torsion angle at the modified dA, in a different duplex with the same

local (-CA**A***G-) sequence context. The two types of conformational equilibria described may occur concurrently in either or both -CA**A***G- oligonucleotides. Although it appears that the existence of multiple conformations may be sequence dependent for both dA (*20*) and dG (*59*) adducts, insufficient data on adducts in different sequence contexts are presently available to assess the importance of such effects.

SUPPORTING INFORMATION AVAILABLE

The NOE distance restraint file and two NOESY contour plots showing connectivities of sugar H2′ and H2″ protons with the base H6/H8 protons for the modified and complementary strands. This material is available free of charge via the Internet at http://pubs.acs.org.

REFERENCES

1. International Agency for Research on Cancer (1983) *Polycyclic Aromatic Compounds*, Part 1, Chemical Environmental and Experimental Data, IARC, Lyon.
2. Jerina, D. M., Cheh, A. M., Chadha, A., Yagi, H., and Sayer, J. M. (1988) in *Microsomes and Drug Oxidations: Proceedings of the 7th International Symposium* (Miners, J. O., Birkett, D. J., Drew, R., May, B. K., and McManus, M. E., Eds.) pp 354−362, Taylor and Francis, London.
3. Jerina, D. M., Chadha, A., Cheh, A. M., Schurdak, M.. E., Wood, A. W., and Sayer, J. M. (1991) in *Biological Reactive Intermediates IV, Molecular and Cellular Effects and Impact on Human Health* (Witmer, C. M., Snyder, R., Jollow, D. J., Kalf, G. F., Kocsis, J. J., and Sipes, I. G., Eds.) pp 533−553, Plenum Press, New York.
4. Thakker, D. R., Yagi, H., Levin, W., Wood, A. W., Conney, A. H., and Jerina, D. M., (1985) in *Bioactivation of Foreign Compounds* (Anders, M. W., Ed.) pp 177−242, New York Academic Press, New York.
5. Buening, M. K., Wislocki, P. G., Levin, W., Yagi, H., Thakker, D. R., Akagi, H., Koreeda, M., Jerina, D. M., and Conney, A. H. (1978) *Proc. Natl. Acad. Sci. U.S.A. 75*, 5358−5361.
6. Slaga, T. J., Bracken, W. J., Gleason, G., Levin, W., Yagi, H., Jerina, D. M., and Conney, A. H. (1979) *Cancer Res. 39*, 67−71.
7. Sayer, J. M., Chadha, A., Agarwal, S. K., Yeh, H. J. C., Yagi, H., and Jerina, D. M. (1991) *J. Org. Chem. 56*, 20−29.
8. Wei, S.-J. C., Chang, R. L., Wong, C. Q., Bhachech, N., Cui, X. X., Hennig, E., Yagi, H., Sayer, J. M., Jerina, D. M., Preston, B. D., and Conney, A. H. (1991) *Proc. Natl. Acad. Sci. U.S.A. 88*, 11227−11230.
9. Wei, S.-J. C., Chang, R. L., Bhachech, N., Cui, X. X., Merkler, K. A., Wong, C.-Q., Hennig, E., Yagi, H., Jerina, D. M., and Conney, A. H. (1993) *Cancer Res. 53*, 3294−3301.
10. Yong, Y., and Romano, L. J. (1996) *Chem. Res. Toxicol. 9*, 179−187.
11. Pommier, Y., Laco, G. S., Kohlhagen, G., Sayer, J. M., Kroth, H., and Jerina, D. M. (2000) *Proc. Natl. Acad. Sci. U.S.A. 97*, 10739−10744.
12. Geacintov, N. E., Cosman, M., Hingerty, B. E., Amin, S., Broyde, S., and Patel, D. J. (1997) *Chem. Res. Toxicol. 10*, 111−146.
13. Cosman, M., de los Santos, C., Fiala, R., Hingerty, B. E., Ibanez, V., Luna, E., Harvey, R. G., Geacintov, N. E., Broyde, S., and Patel, D. J. (1993) *Biochemistry 32*, 4145−4155.
14. Cosman, M., Hingerty, B. E., Ibanez, V., Luneva, N., Amin, S., Geacintov, N. E., Broyde, S., and Patel, D. J. (1996) *Biochemistry 35*, 9850−9863.
15. Cosman, M., de los Santos, C., Fiala, R., Hingerty, B. E., Singh, S. B., Ibanez, V., Margulis, L. A., Live, D., Geacintov, N. E., Broyde, S., and Patel, D. J. (1992) *Proc. Natl. Acad. Sci. U.S.A. 89*, 1914−1918.
16. De los Santos, C., Cosman, M., Hingerty, B. E., Ibanez, V., Margulis, L. A., Geacintov, N. E., Broyde, S., and Patel, D. J. (1992) *Biochemistry 31*, 5245−5252.
17. Schurter, E. J., Sayer, J. M., Oh-hara, T., Yeh, H. J. C., Yagi, H., Luxon, B. A., Jerina, D. M., and Gorenstein, D. G. (1995) *Biochemistry 34*, 9009−9020.
18. Schurter, E. J., Yeh, H. J. C., Sayer, J. M., Lakshman, M. K., Yagi, H., Jerina, D. M., and Gorenstein, D. G. (1995) *Biochemistry 34*, 1364−1375.
19. Zegar, I. S., Kim, S. J., Johansen, T. N., Horton, P. J., Harris, C. M., Harris, T. M., and Stone, M. P. (1996) *Biochemistry 35*, 6212−6224.
20. Zegar, I. S., Chary, P., Jabil, R. J., Tamura, P. J., Johansen, T. N., Lloyd, R. S., Harris, C. M., Harris, T. M., and Stone, M. P. (1998) *Biochemistry 37*, 16516−16528.
21. Volk, D. E., Rice, J. S., Luxon, B. A., Yeh, H. J. C., Liang, C., Xie, G., Sayer, J. M., Jerina, D. M., and Gorenstein, D. G. (2000) *Biochemistry 39*, 14040−14053.
22. Mao, B., Gu, Z., Gorin, A., Chen, J., Hingerty, B. E., Amin, S., Broyde, S., Geacintov, N. E., and Patel, D. J. (1999) *Biochemistry 38*, 10831−10842.
23. Yeh, H. J. C., Sayer, J. M., Liu, X., Altieri, A. S., Byrd, R. A., Lakshman, M. K., Yagi, H., Schurter, E. J., Gorenstein, D. G., and Jerina, D. M. (1995) *Biochemistry 34*, 13570−13581.
24. Lakshman, M. K., Sayer, J. M., Yagi, H., and Jerina, D. M. (1992) *J. Org. Chem. 57*, 4585−4590.
25. States, D. J., Haberkorn, R. A., and Ruben, D. J. (1982) *J. Magn. Reson. 48*, 286−292.
26. Bax, A., and Davis, D. G. (1985) *J. Magn. Reson. 65*, 355−360.
27. Braunschweiler, L., and Ernst, R. R. (1983) *J. Magn. Reson. 53*, 521−528.
28. Jeener, J., Meier, B. H., Bachmann, P., and Ernst, R. R. (1979) *J. Chem. Phys. 71*, 4546−4553.
29. Kumar, A., Ernst, R. R., and Wuthrich, K. (1980) *Biochem. Biophys. Res. Commun. 95*, 1−6.
30. Zhang, S., Yang, X., and Gorenstein, D. G. (2000) *J. Magn. Reson. 143*, 382−386.
31. Ogg, R. J., Kingsley, P. B., and Taylor, J. S. (1994) *J. Magn. Reson. 104*, 1−10.
32. Tomasz, M., Olson, J., and Mercado, C. M. (1972) *Biochemistry 11*, 1235−1241.
33. Bullock, F. J., and Jardetzky, D. (1964) *J. Org. Chem. 29*, 1988−1990.
34. Bothner-By, A., Stephen, R. L., and Lee, J.-M. (1984) *J. Am. Chem. Soc 106*, 811−813.
35. Bax, A., and Davis, D. G. (1985) *J. Magn. Reson. 63*, 207−213.
36. Weiner, S. J., Kollman, P. A., Case, D. A., Singh, U. C., Ghio, C., Alagona, G., Profeta, S., Jr., and Weiner, P. (1984) *J. Am. Chem. Soc. 106*, 765−784.
37. Weiner, S. J., Kollman, P. A., Nguyen, D. T., and Case, D. A. (1986) *J. Comput. Chem. 7*, 230−252.
38. Hingerty, B. E., and Broyde, S. (1985) *Biochemistry 24*, 2279−2299.
39. Wuthrich, K. (1986) *NMR of Proteins and Nucleic Acids*, Wiley, New York.
40. Searle, M. S. (1993) in *Progress in NMR Spectroscopy* (Emsley, J. W., Feeney, J., and Sutcliffe, L. H., Eds.) Vol. 25, pp 403−480, Pergamon Press, London.
41. Saenger, W. (1984) *Principles of Nucleic Acid Structure*, pp 266−267, Springer, New York.
42. Boelens, R., Koning, T. M. G., van Brom, J. H., and Kaptein, R. (1988) *J. Mol. Struct. 173*, 299−311.
43. Boelens, R., Koning, T. M. G., van der Marel, G. A., and Kaptein, R. J. (1989) *J. Magn. Reson. 82*, 290−308.
44. Gonzalez, C., Rullmann, J. A. C., Bonvin, A. M. J. J., Boelens, R., and Kaptein, R. (1991) *J. Magn. Reson. 91*, 659−664.
45. Reid, B. R. (1987) *Q. Rev. Biophys. 20*, 1−34.
46. Patel, D. J., Shapiro, L., and Hare, D. (1987) *Q. Rev. Biophys. 20*, 35−112.

47. Sayer, J. M., Shah, J. H., Liang, C., Xie, G., Kroth, H., Yagi, H., Liu, X., Yeh, H. J. C., and Jerina, D. M. (2000) *Polycyclic Aromat. Compd. 17*, 95−104.
48. Cosman, M., Laryea, A., Fiala, R., Hingerty, B. E., Amin, S., Geacintov, N. E., Broyde, S., and Patel, D. J. (1995) *Biochemistry 34*, 1295−1307.
49. Li, Z., Kim., H.-Y., Tamura, P. J., Harris, C. M., Harris, T. M., and Stone, M. P. (1999) *Biochemistry 38*, 16045−16057.
50. Cosman, M., Fiala, R., Hingerty, B. E., Laryea, A., Lee, H., Harvey, R. G., Amin, S., Geacintov, N. E., Broyde, S., and Patel, D. J. (1993) *Biochemistry 32*, 12488−12497.
51. Li, Z., Mao, H., Kim, H.-Y., Tamura, P. J., Harris, C. M., Harris, T. M., and Stone, M. P. (1999) *Biochemistry 38*, 2969−2981.
52. Lavery, R., and Sklenar, H. J. (1988) *J. Biomol. Struct. Dyn. 6*, 63−91.
53. Dickerson, R. E., and Drew, H. R. (1981) *J. Mol. Biol. 149*, 761−786.
54. Shui, X. Q., McFail-Isom, L., Hu, G. G., and Williams, L. D. (1998) *Biochemistry 37*, 8341−8355.
55. Tjandra, N., Tate, S. I., Ono, A., Kainosho, M., and Bax, A. (2000) *J. Am. Chem. Soc. 122*, 6190−6200.
56. Kabsch, W., Snader, C., and Trifonov, E. N. (1982) *Nucleic Acids Res*. 1097−1104.
57. Tan, J., Geacintov, N. E., and Broyde, S. (2000) *J. Am. Chem. Soc. 122*, 3021−3032.
58. Schwartz, J. L., Rice, J. S., Luxon, B. A., Sayer, J. M., Xie, G., Yeh, H. J. C., Liu, X., Jerina, D. M., and Gorenstein, D. G. (1997) *Biochemistry 36*, 11069−11076.
59. Fountain, M. A., and Krugh, T. R. (1995) *Biochemistry 34*, 3152−3161.

BI002896Q